ACS APPLIED MATERIALS & INTERFACES

Research Article

www.acsami.org

Preparation of Hollow *N*-Chloramine-Functionalized Hemispherical Silica Particles with Enhanced Efficacy against Bacteria in the Presence of Organic Load: Synthesis, Characterization, and Antibacterial Activity

Hakim Rahma,[†] Sogol Asghari,[†] Sarvesh Logsetty,[‡] Xiaochen Gu,[§] and Song Liu*[,†,∥,⊥,#]

[†]Departments of Textile Sciences, [‡]Surgery, [∥]Biosystems Engineering, [⊥]Medical Microbiology, and [#]Chemistry, University of Manitoba, Winnipeg, Manitoba R3T 2N2, Canada

[§]College of Pharmacy, University of Manitoba, Winnipeg, Manitoba R3E 0T5, Canada

Supporting Information

ABSTRACT: The fabrication of highly effective antimicrobial materials is an important strategy for coping with the growing concern of bacterial resistance. In this study, *N*-chloramine-functionalized hollow hemispherical structures were designed and prepared to examine possible enhancement of antimicrobial performance. Antimicrobial testing was carried out on Gram-negative *(Escherichia coli)* and Gram-positive *(Baccilus Cereus)* bacteria in the presence and absence of biological medium. The efficacy of the hollow hemispherical particles functionalized with various *N*-chloramines in killing bacteria was compared among themselves with that of small organic molecules and spherical particles to investigate the effect of the surface charge, chemical structure, and shape of the particles. Results demonstrated that quaternary ammonium salt or amine functions in the chemical structure enhanced the antimicrobial activity of the particles and made the particles more effective than the small molecules in the presence of biological medium. The importance of particle shape in the killing tests was also confirmed.

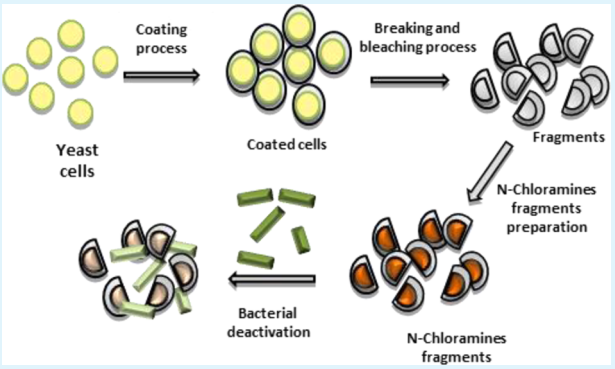

KEYWORDS: *antibacterial, silica, N-chloramine, hollow hemispherical structure, positive charge*

INTRODUCTION

Bacterial resistance to antibiotics has been increasing over the years; there is a strong need for the development of new antimicrobial materials with broader efficiencies to reduce antibiotic usage and to minimize potential biological resistance.[1−3] Of all broad-spectrum biocides, *N*-chloramine compounds are considered to be the most powerful biocidal agents due to the $\delta+$ oxidation state of chlorine in the N−Cl bond of *N*-chloramine, which is capable of attacking multiple targets of bacterial cells and causing irreversible damage.[4] Additionally, organic *N*-chloramines possess desirable antibacterial properties, including high durability in water, long-term stability, and regenerability.[4] They are also less likely to induce bacterial resistance.[4]

The antimicrobial efficiency of *N*-chloramine-based materials is strongly dependent on the contact surface area and contact time of the microorganisms with the chemicals.[5−7] Chen et al.[6] reported enhancement of an antimicrobial effect from *N*-chloramine-functionalized particles when compared to bulk *N*-chloramine material and attributed the enhancement to an increase in the contact surface area of the particles. Using yeast cells as a template, Borovička et al.[8,9] prepared hollow hemispherical silica microparticles coated with gold on their internal side (concave surface). The resultant particles demonstrated selective and effective killing of yeast upon laser irradiation. It was estimated that the interaction energy between a spherical yeast cell and the inner side of the hollow hemispherical silica particle could be 1000× higher than that with the outer side.[9] Hence, the immobilization of biocidal compounds on inorganic-based materials could provide an ordered structure with improved antimicrobial properties against bacteria and fungi.

Silica particles are one of the most extensively used supporting materials in biological applications. They are biocompatible, chemically inert, and water dispersible;[10] silanol groups on the silica surface also offer versatile possibilities for covalently functionalizing the silica-coated particles.[11] Synthesis attempts have been made to incorporate *N*-chloramine compounds onto the silica surface[12−16] either in the form of silica gel (noncontrolled morphology) via sol−gel chemistry of

Received: March 20, 2015
Accepted: May 5, 2015
Published: May 5, 2015

DOI: 10.1021/acsami.5b02486
ACS Appl. Mater. Interfaces 2015, 7, 11536−11546

Stöber poly condensation or through a one step S_N2 reaction with the chloro functional group previously introduced by condensing 3-chloropropyl trimethoxysilane to the surface of silica. The silanol groups on the silica surface serve as a base to anchor the *N*-chloramine silane precursors.

Although *N*-chloramine silica particles exhibit many desirable features, a variety of organic loads (e.g., wound exudate, blood sera, or extracellular matrices) may decrease the antimicrobial efficacy of *N*-chloramine, thus compromising clinical use of these materials.[17,18] Kloth et al.[17] used chloramine T as an antiseptic for wound disinfection and compared the antimicrobial efficiency of the compound on *Escherichia coli* and *Pseudomonas aeruginosa* in the presence of fetal bovine serum (FBS); the presence of proteins in the medium reduced the antimicrobial effect of chloramine T due to interference between the compound and the proteins. We have reported that a positive charge covalently attached to a planar support (fabric) helped to boost the antimicrobial properties of the *N*-chloramine materials.[19] Because both Gram-positive and Gram-negative bacteria are negatively charged owing to the presence of teichoic acid and phosphate on their membrane and cell wall, adding a positive charge on a support would attract the bacteria and hence allow for a faster oxidative chlorine transfer to the target sites. The other approach to decreasing the quenching of *N*-chloramine by the proteins is to modulate the chemical functions of the compounds depending on the intended purpose.[4] The *N*-chloramines can be structurally categorized into three types: imide (−C(═O)−NCl−C(═O)−), amide (C(═O)−NCl−), and amine (R−NCl).[20] The stability of the N−Cl bond against hydrolysis depends on the function and follows the order imide < amide < amine, whereas their antimicrobial activity follows the inverse trend of imide > amide > amine. Both stability and activity characteristics are useful in selecting an ideal antimicrobial substance to serve the intended biological application.

In this study, we focused on the synthesis of the *N*-chloramine-functionalized hollow hemispherical silica particles and subsequent characterization of the antibacterial properties. It was hypothesized that an increase in the contact surface between the antibacterial material and the bacteria would enhance the biocidal efficacy of the test material. These materials were prepared by the sol−gel method using yeast cells as a template; the physical and chemical properties of the resulting materials were examined by SEM/EDX, FT-IR, and zeta potential measurements, and their antimicrobial efficacy was studied in phosphate buffered solutions (PBS) and protein-enriched medium to evaluate the effect of chemical structures, surface charges, and the shape of the particles on their resistance to protein quenching.

MATERIALS AND METHODS

Chemicals and Reagents. All solvents and chemicals, such as tetraethylorthosilicate (TEOS), (3-aminopropyl)triethoxysilane (APTES), (3-chloropropyl)triethoxysilane (CPTES), and 5,5-dimethylhydantoin, were purchased from either Aldrich or Fisher and used without further purification unless otherwise noted; yeast were obtained from a local food store. MacConkey agar, MacConkey broth, Nutrient agar, and Nutrient broth were purchased from Becton Dickinson and Company. Fibroblast Basal Medium (FBM) (PCS-201-030) was purchased from ATCC.

Instrumentation. SEM images were collected using a JEOL-5900LV field emission scanning electron microscope. Energy-dispersive X-ray (EDX) data was also recorded during the scanning electron microscope measurements. FT-IR spectra were recorded on a Thermo Nicolet iS10 FT-IR Spectrometer. Zeta potential (0.1 mg/mL of fragment suspension; Smoluchowski mode) was determined by dynamic light scattering using a Brookhaven ZetaPALS potential analyzer. NMR spectra were acquired at room temperature in 5 mm NMR tubes on a Bruker Avance 300 MHz NMR spectrometer. Accurate mass spectra were acquired using a PerkinElmer prOTOF 2000 MALDI-OTOF mass spectrometer.

Synthesis of SiO_2 Particles. The coating was performed according to the Stöber Process. Briefly, 6 g of baker's yeast cells were suspended in 12 mL ethanol/water (1:1) solution, and 1 mL of 25% ammonia was added as the catalyst followed by 9 g of TEOS. The suspension was stirred at room temperature for 3 h. Solid precipitates were recovered by centrifugation (2 min, 3000 rpm), washed 3 times with ethanol, and 3 times with distilled water. The particles were then dried at 110 °C overnight.

Synthesis of CPTES@SiO_2 and CPTES/SiO_2@SiO_2 Particles. Six grams of yeast cells were suspended in 6 mL of ethanol and 6 mL of 25% ammonia. Subsequently, CPTES and TEOS (CPTES@SiO_2: 3g of CPTES; CPTES/SiO_2@SiO_2: 1.6 g of CPTES, 2 g of TEOS) were added to the suspension, and the mixture stirred continuously for 3 h. Afterwards, the product was centrifuged (2 min, 3000 rpm), washed 3 times with ethanol, and 3 times with distilled water. The particles were resuspended in 6 mL of ethanol and 6 mL distilled water, followed by the addition of 1 mL of ammonia and 5 g of TEOS. The suspension was stirred for another 3 h, centrifuged, and washed as before. The particles were then dried at 110 °C overnight.

Fragmentation and the Bleaching Process. SiO_2, CPTES@SiO_2, and CPTES/SiO_2@SiO_2 particles were fragmented as follows: 3 g of particles were placed in a glass cylinder and 30 mL of concentrated sulfuric acid was added slowly. The mixture was stirred with a glass rod to produce a homogeneous suspension, and the container was placed in an ultrasonic bath (10 min for CPTES@SiO_2 and CPTES/SiO_2@SiO_2 and 25 min for SiO_2). An aliquot of ice water was slowly added to dilute the suspension. The solid residues were then recovered by centrifugation (2 min, 3000 rpm), washed 3 times with distilled water, and 4 times with ethanol. A bleach solution was prepared by diluting commercial bleach (1:3) and adjusting the pH to 8 using hydrochloric acid. The fragments were then washed twice with the bleach solution and rinsed 4 times with distilled water. The solid particles were centrifuged and dried at 70 °C for 2 h.

Synthesis of DMH$^-$K$^+$. Eight grams (62.4 mmol) of 5,5-dimethyl hydantoin, 4.12 g (62.4 mmol) of potassium hydroxide, and 40 mL of ethanol were added to a round-bottom flask. The solution was stirred and heated at reflux for 2 h, followed by evaporation and drying of the solvent under vacuum for 16 h.

Synthesis of DMH−CH_2−$N(CH_3)_2$. To 20 mL of methanol in a round-bottom flask were added 6.6 grams (0.05 mol) of 5,5-dimethyl hydantoin, 4.1 g of dimethylamine hydrochloride, 4 mL of formaldehyde (37%); then, 2 g of sodium hydroxide was added to the mixture, and the solution was stirred at room temperature for 2 h. The organic solvent was subsequently evaporated under a vacuum. The residual product was diluted with water and extracted with ethyl acetate. The organic phase was then evaporated and dried under vacuum to produce 4.7 g of pure product (25.4 mmol, 51% yield).

^{1}H NMR ($CDCl_3$, 300 MHz) δ 4.32 (s, 2H), 2.29 (s, 6H), 1.41(s, 6H); ^{13}C NMR ($CDCl_3$, 75 MHz) δ 178.6, 157.4, 60.7, 58.8, 42.7, 25.2; HRMS (MALDI-TOF) m/z [M + H]$^+$ calcd for $C_8H_{16}N_3O_2^+$ 186.1237, found 186.1185.

Synthesis of DMH-$(CH_2)_3$-$N(CH_3)_2$. To 100 mL of ethanol in a round-bottom flask were added 4.8 g (19.26 mmol) of DMH-$(CH_2)_3$-Br, 7.63 g (0.122 mol) of potassium hydroxide, 7.85 g (96.3 mmol) of dimethylamine hydrochloride; then, the suspension was heated at reflux overnight. The organic solvent was evaporated under vacuum, and the resultant product extracted with dichloromethane, dried, and concentrated to produce 2 g of product at 50% yield.

^{1}H NMR (D_2O, 300 MHz) δ 3.55 (t, J = 7.5 Hz, 2H), 2.65 (t, J = 7.5 Hz, 2H), 2.46 (s, 6H; $N(CH_3)_2$), 1.89(m, 2H), 1.44 (s, 6H); ^{13}C NMR (D_2O, 75 MHz) δ 180.8, 157.3, 59.1, 55.4, 43.3, 36.1, 24.2, 23.4; HRMS (MALDI-TOF) m/z [M + H]$^+$ calcd for $C_{10}H_{20}N_3O_2^+$ 214.1550, found 214.1549.

DOI: 10.1021/acsami.5b02486
ACS Appl. Mater. Interfaces 2015, 7, 11536−11546

Scheme 1. Synthesis of SiO_2 and CPTES/SiO_2@SiO_2 Fragments

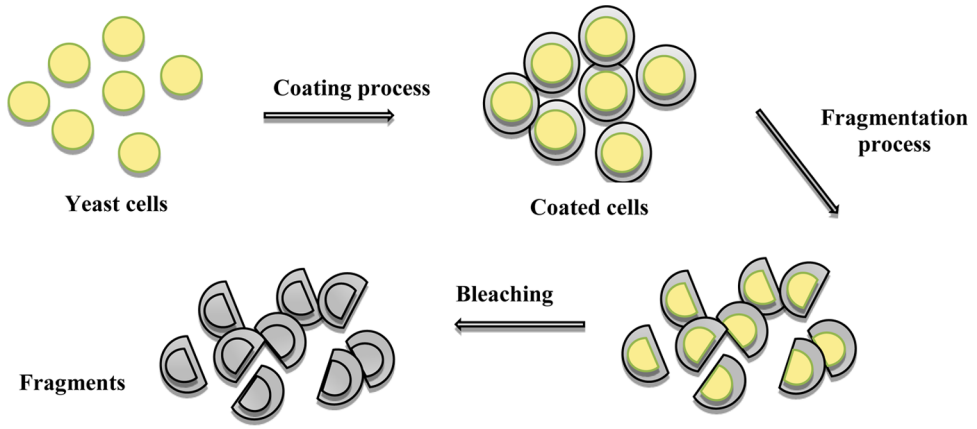

Synthesis of DMH-$(CH_2)_3$-$N^+(CH_3)_3Cl^-$. To the solution of DMH-$(CH_2)_3$-Br (1.0 g, 4.0 mmol) in EtOH (5 mL) was added aqueous dimethylamine (2.2 mL, 24 wt %, 8.0 mmol) at room temperature. The resulting solution was heated to reflux overnight. The removal of the solvent and the excess dimethylamine was carried out under reduced pressure. The crude product was then dissolved in a minimum amount of water and slowly passed through an anion-exchange resin (Amberlite R IRA-900, Cl^-) to give the product as a white solid (0.94g, 90%).

^{1}H NMR (D_2O, 300 MHz) δ 3.63 (t, J = 6.9 Hz, 2H), 3.41 (t, J = 8.4 Hz, 2H), 3.18 (s, 9H), 2.17 (m, 2H), 1.46 (s, 6H); ^{13}C NMR (D_2O, 75 MHz) δ 180.6, 157.1, 63.8, 69.2, 53.0, 35.4, 23.5, 21.7; HRMS (MALDI-TOF) m/z [M − Cl]$^+$ calcd for $C_{11}H_{22}N_3O_2^+$ 228.1707, found 228.1704.

Synthesis of DMH-$(CH_2)_2$-OH. To 6.4 g (46.3 mmol) of anhydrous K_2CO_3 in 160 mL acetone was added 1.96 g (15.5 mmol) of 5,5-dimethyl hydantoin. The reaction mixture was heated to gentle reflux for 30 min, and 1.6 mL (22.6 mmol) of 2-bromoethanol was added. The reflux was continued for 6 h, the solution filtered off, and the solvent removed. The crude product was purified by column chromatography (ethyl acetate/hexane, 4:1, v/v) to afford the product as a white solid (2.2 g, 81%).

^{1}H NMR ($CDCl_3$, 300 MHz) δ 3.76 (t, J = 5.4 Hz, 2 H), 3.65 (t, J = 5.4 Hz, 2 H), 1.45 (s, 6 H); ^{13}C NMR ($CDCl_3$, 75 MHz) δ 178.1, 157.2, 60.5, 59.1, 41.6, 24.9; HRMS (MALDI-TOF) m/z [M + H]$^+$ calcd for $C_7H_{13}N_2O_3^+$ 173.0921, found 173.0907.

Synthesis of DMH@SiO_2 Fragments. Four grams of CPTES/SiO_2@SiO_2 fragments and 4 g of DMH^-K^+ were mixed in 20 mL of DMF. The suspension was stirred and heated at 100 °C overnight. The resulting residual fragments were centrifuged for 2 min at 3000 rpm, washed 3 times with distilled water, and washed 3 times with ethanol. The fragments were then dried at 70 °C for 2 h.

Synthesis of DMHQAS1C@SiO_2 and DMHQAS3C@SiO_2 Fragments. CPTES/SiO_2@SiO_2 fragments (2.7 and 4 g, respectively) and DMH-$(CH_2)_n$-$N(CH_3)_2$ (n = 1:3 g; n = 3:5.12 g) were mixed in DMF; potassium bromide was added (1.5 and 2.9 g, respectively), and the suspension was heated at 110 °C overnight. The resulting DMHQAS1C@SiO_2 and DMHQAS3C@SiO_2 fragments were recovered by centrifugation (2 min, 3000 rpm), washed 3 times with distilled water, and washed 5 times with ethanol. The fragments were then dried at 70 °C for 2 h.

Synthesis of Amine@SiO_2 Fragments. Four grams of CPTES/SiO_2@SiO_2 fragments and 8 mL of ethylene diamine were mixed in 20 mL of DMF; then, 2.9 g of potassium bromide was added to the mixture. The suspension was stirred and heated at 110 °C overnight. The residual fragments were then centrifuged (2 min, 3000 rpm), washed 3 times with distilled water, and washed 3 times with ethanol. The fragments were then dried at 70 °C for 2 h.

Synthesis of DendAmine@SiO_2 Fragments. In 20 mL of methanol were mixed 2.5 g of Amine@SiO_2 fragments and 15 mL of methyl acrylate. The suspension was stirred at 50 °C for 3 days. The resulting fragments were then washed 5 times with ethanol and dried at 70 °C for 2 h. The resulting fragments were added to an Erlenmeyer flask. Fifteen milliliters of methanol and 15 mL of ethylene diamine were then added. The suspension was stirred at room temperature for 5 days; then, the resultant DendAmine@SiO2 was dried at 70 °C for 2 h.

Chlorination of All Particle Fragments. One gram of the fragments was suspended in 10 mL of *tert*-butyl alcohol. The suspension was immersed in an ultrasonic bath for 30 s, followed by the addition of 3 mL of *tert*-butyl hypochlorite and stirred at room temperature overnight. The resulting fragments were then washed once with *tert*-butyl alcohol, rinsed 5 times with ethanol and dried at 55 °C for 2 h.

Synthesis of Compound 1 (C1) and Compound 2 (C2). To the solution of nonchlorinated compound (DMH-$(CH_2)_2$-OH or DMH-$(CH_2)_3$-$N^+(CH_3)_3Cl^-$) in mixed solvent (*t*-BuOH/H_2O, 4:1, v/v) was added 3 equiv of excess *tert*-butyl hypochlorite. The reaction was allowed to stir thoroughly for 22−24 h. Excessive *tert*-butyl hypochlorite and solvent were removed under vacuum, and the corresponding chlorinated forms (**C1** and **C2**) were thus obtained as white solids.

*Compound 1 (**C1**).* ^{1}H NMR ($CDCl_3$, 300 MHz) δ 3.78−3.84 (m, 4 H), 1.50 (s, 6 H); ^{13}C NMR ($CDCl_3$, 75 MHz) δ 174.9, 154.9, 66.1, 60.3, 42.4, 22.2; HRMS (MALDI-TOF) m/z [M + H]$^+$ calcd for $C_7H_{12}ClN_2O_3^+$ 207.0531, found 207.0517.

*Compound 2 (**C2**).* ^{1}H NMR (D_2O, 300 MHz) δ 3.69 (t, J = 6.9 Hz, 2H), 3.43−3.38 (m, 2H), 3.15 (s, 9H), 2.22−2.12 (m, 2H), 1.51 (s, 6H); ^{13}C NMR ($CDCl_3$, 75 MHz) δ 181.8, 160.4, 71.3, 68.7, 58.0, 41.6, 26.6, 25.9; HRMS (MALDI-TOF) m/z [M − Cl]$^+$ calcd for $C_{11}H_{21}ClN_3O_2^+$ 262.1317, found 262.1317.

Antimicrobial Testing in PBS or Cell Culture Medium. Nutrient agar was used for the *B. cereus* culture and McConkey agar was used for *E. coli*. After being cultured on agar plates, the logarithmic-phase cultures were initially prepared by suspending several colonies in PBS (pH 7.4, 0.05M) at a density equivalent to a 0.5 McFarland standard. The *E. coli* suspension was diluted 100×, whereas the *B. cereus* solution was not diluted. Twenty microliters of the diluted *E. coli* and *B. cereus* suspensions were further diluted into 60 mL of McConkey and Nutrient broth, respectively. After culturing the bacteria in an incubator at 37 °C for 18 h, the concentration of *E. coli* went up to 10^8 CFU/mL and that of *B. Cereus* to 5×10^6 CFU/mL. The suspensions were again diluted by 1000× and 50×, respectively, yielding a starting inoculum of 10^5 CFU/mL (20 mL total volume). For antimicrobial testing in PBS, only PBS was used for the dilutions. In the case of killing tests in FBM medium, 50% PBS and 50% FBM were used for diluting the bacterial solutions. To maintain identical chlorine content in all testing samples, the amounts of fragments and organic molecules were calculated based on the titration results (m_{Cl} = 0.02 mg). The testing samples were placed in sterile tubes, and 2 mL of the bacterial suspension was then added to the samples. The mixtures were sonicated for 10 s, vortexed, and then

DOI: 10.1021/acsami.5b02486
ACS Appl. Mater. Interfaces 2015, 7, 11536−11546

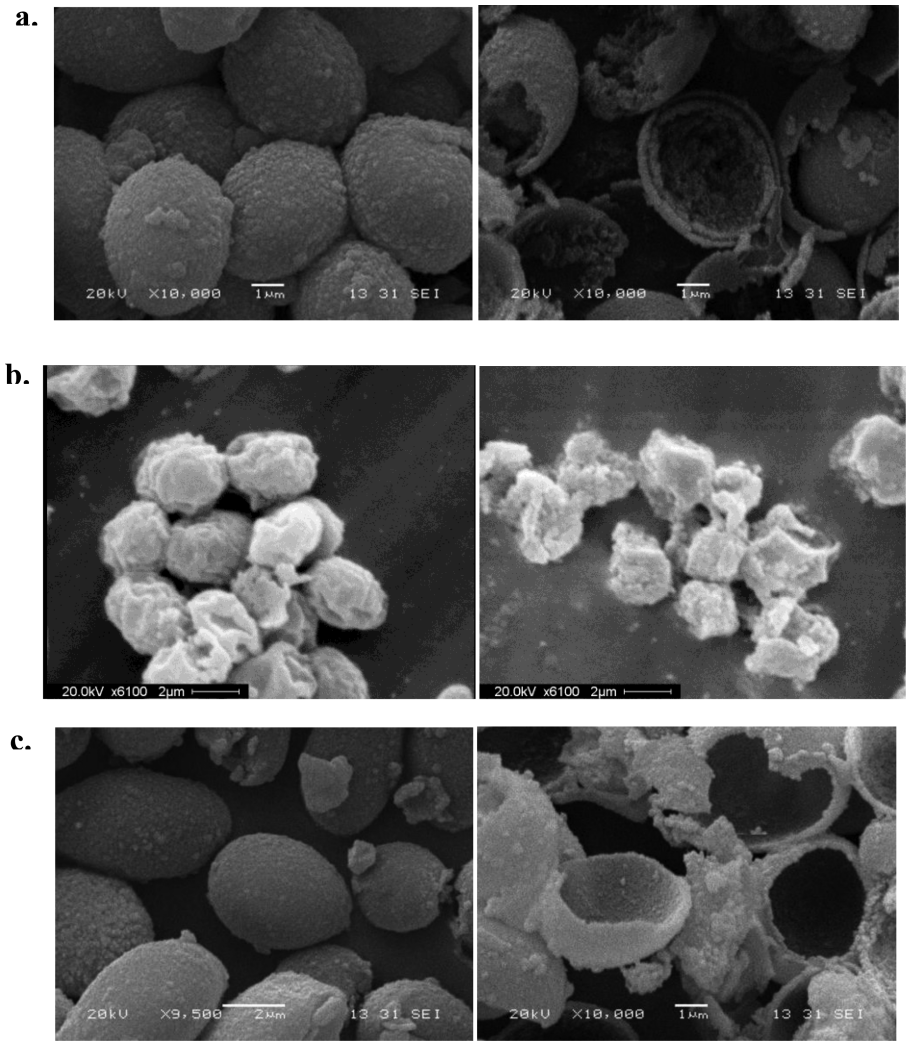

Figure 1. SEM images of the particles (left, after coating; right, after fragmentation and removal of yeast): (a) yeast@SiO_2 and hemispheric SiO_2 shell, (b) yeast@CPTES@SiO_2 and CPTES@SiO_2 shell, and (c) yeast@CPTES/SiO_2@SiO_2 and hemispheric CPTES/SiO_2@SiO_2 shell.

shaken (Twist shaker) for the duration of the experiment. After the contact had reached a predetermined time interval, 100 μL of cell suspension was withdrawn; 0.9 mL of PBS and 50 μL of 1 N sodium thiosulfate were then added to quench the bactericidal effect. The quenched suspension was then serially diluted in PBS (10× less concentrated than the previous one), and 100 μL of each dilution was placed onto the agar plates. The same procedures were applied to the blanks as the controls with the same matrices but without actual samples. The bacterial colonies on the agar plates were enumerated after being incubated at 37 °C for 24 h.

$$\text{Percent reduction of bacteria (\%)} = (A - B)/A \times 100;\ \log(\text{reduction}) = \log(A/B)$$

where A is the number of bacterial colonies in the control (CFU/mL), and B is the number of bacterial colonies under the effect of the synthesized compounds.

RESULTS AND DISCUSSION

Synthesis and Characterization of the Fragments. Scheme 1 depicts the synthesis strategy of the hollow hemispherical particles. Fabrication of the fragments was achieved by adapting the method reported by Borovička et al.[8] The synthesis was based on the Stöber Reaction (i.e., the formation of inorganic silica layer on the template (*Saccharomyces cerevisiae*)); this was followed by the fragmentation of the hollow particles using concentrated sulfuric acid and ultrasonication and the removal of cell cores through bleaching. Initial attempts were also made using one-step coating and functionalization by synthesizing 1-(3-(4,4-dimethyl-2,5-dioxoimidazolidin-1-yl)propyl)-3-(3-(triethoxysilyl) propyl) urea and 3-(4,4-diethoxy-10-hydroxy-3,8-dioxa-12-aza-4-silapentadecan-15-yl)-5,5-dimethylimidazolidine-2,4-dione. However, it was impossible to polymerize either of the above functional triethoxysilanes onto the yeast cells, partially because of steric hindrance of the bulk molecular structures. Subsequently, a two-step coating and functionalization strategy was adopted. A functional silane (3-chloropropyltriethoxysilane, CPTES) was first used to coat the yeast cell; TEOS was then deposited to the CPTES coating for shielding. After breaking the resulting particle and scarifying the yeast template, the chloropropyl functional group on the inner CPTES layer was further derivatized into various *N*-chloramine precursors. When CPTES was introduced to the structure, it changed the mechanical and physical properties of the particles; hence, a synthesis optimization step was required. The fragmentation process was also found to be technically challenging because this process needs to fragment the silica coating without

DOI: 10.1021/acsami.5b02486
ACS Appl. Mater. Interfaces 2015, 7, 11536−11546

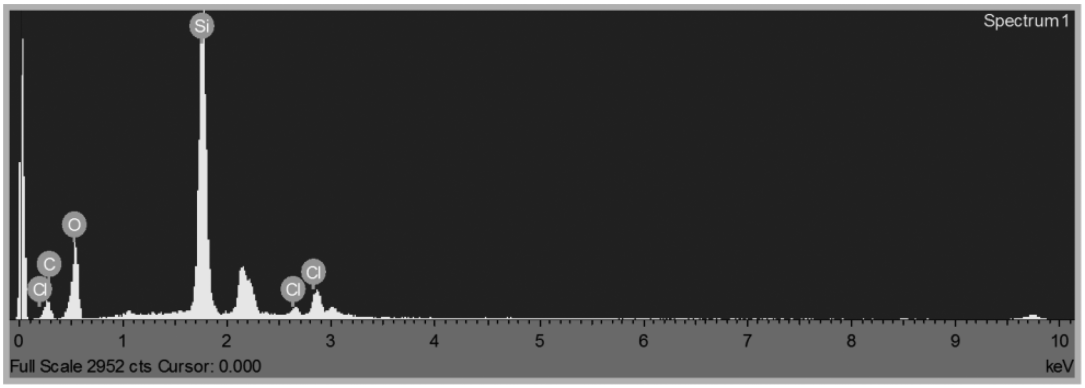

Figure 2. EDX spectrum of CPTES/SiO_2@SiO_2 fragments.

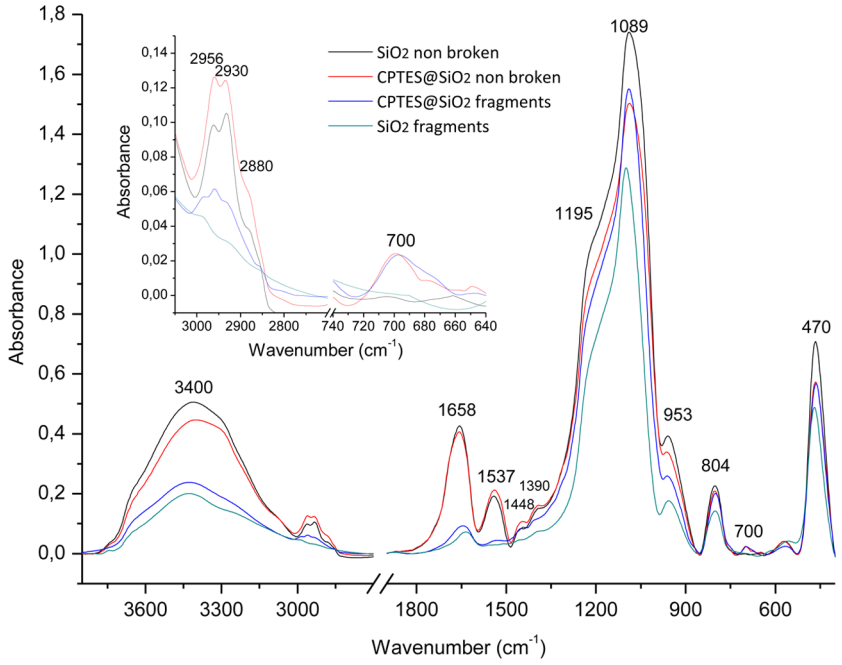

Figure 3. FT-IR spectra of SiO_2, CPTES/SiO_2@SiO_2, and their fragments.

damaging the introduced chloropropyl functional group. The previously reported fragmentation[8] effected by a harsh Piranha solution (3:1 concentrated sulfuric acid and hydrogen peroxide) was not applicable because this solution would destroy all of the organic substances.

The morphology of the samples after the coating and fragmentation was observed using SEM (Figure 1). Silica particles free of functional silane (CPTES) were used as a reference for the quality control of the fragmentation process (Figures S1 and S2 in the Supporting Information). Figure 1a shows a representative SEM image of the coated yeast cells with the silica layer, which exhibited monodisperse, well-defined, homogeneously coated spherical particles with an average diameter of 4.5 ± 0.7 μm. The fragmentation of the silica-coated particles led to the formation of homogeneous half-spherical structures (SiO_2 fragments), and the shell thickness ranged from approximately 100 to 150 nm.

To introduce CPTES into the structure, the coating procedure comprised two steps (i.e., hydrolysis condensation of CPTES on the yeast cells followed by hydrolysis condensation of TEOS). The SEM images (Figure 1b) show not very well-defined rough coating surfaces. To avoid damage to the introduced chloropropyl functional group, a milder fragmentation method was utilized by combining concentrated sulfuric acid with sonication. Nevertheless, the fragmentation of these particles (CPTES@SiO_2 fragments) still produced completely collapsed fragments, possibly due to the soft structure generated by the low-density polysiloxane network.

To rigidify the structure, we simultaneously added TEOS to CPTES during the first coating stage; the polycondensation of TEOS with CPTES consequently increased the interconnectivity of the network, resulting in stronger structures. Afterwards, a second layer of TEOS was added to further cover the first layer. The resultant SEM images (Figure 1c) show a well-defined structure with a smooth surface and a surface morphology similar to that of the SiO_2 particles (Figures S3 and S4 in the Supporting Information). It was apparent that the fragmentation of the particles (CPTES/SiO2@SiO_2 fragments) produced well-defined hemispherical fragments. To yield a noncollapsed spherical structure after the fragmentation process with sulfuric acid, a properly cross-linked polysiloxane network would be necessary.

EDX spectrum in Figure 2 shows the compositional information on CPTES/SiO_2@SiO_2, indicating the presence

DOI: 10.1021/acsami.5b02486
ACS Appl. Mater. Interfaces 2015, 7, 11536−11546

Scheme 2. Synthesis of the *N*-Chloramine Fragment Precursors Used in the Study

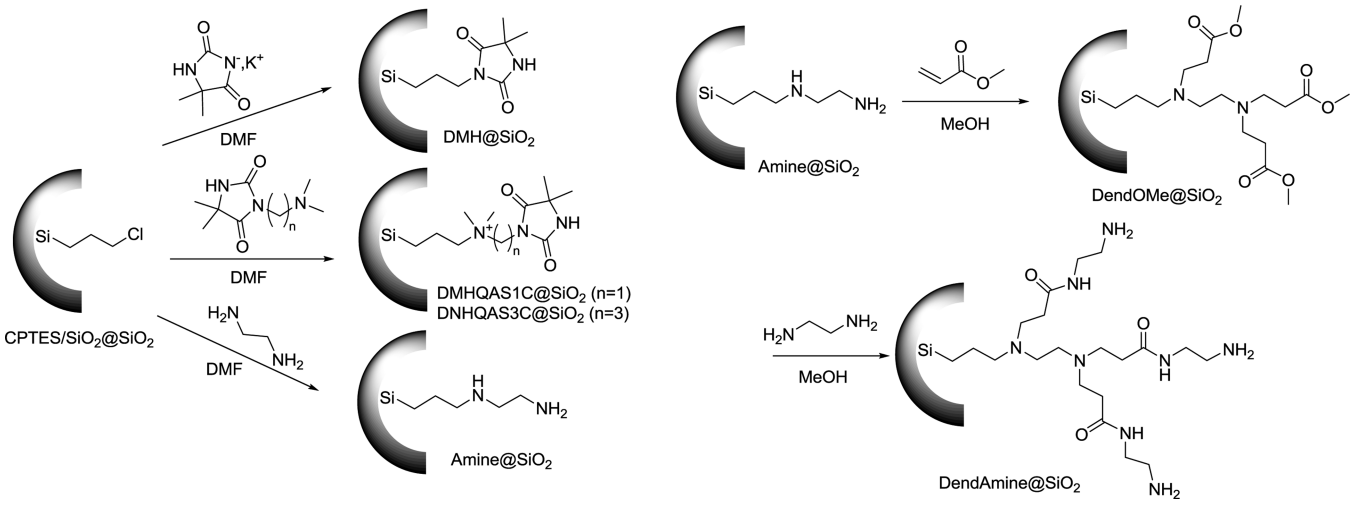

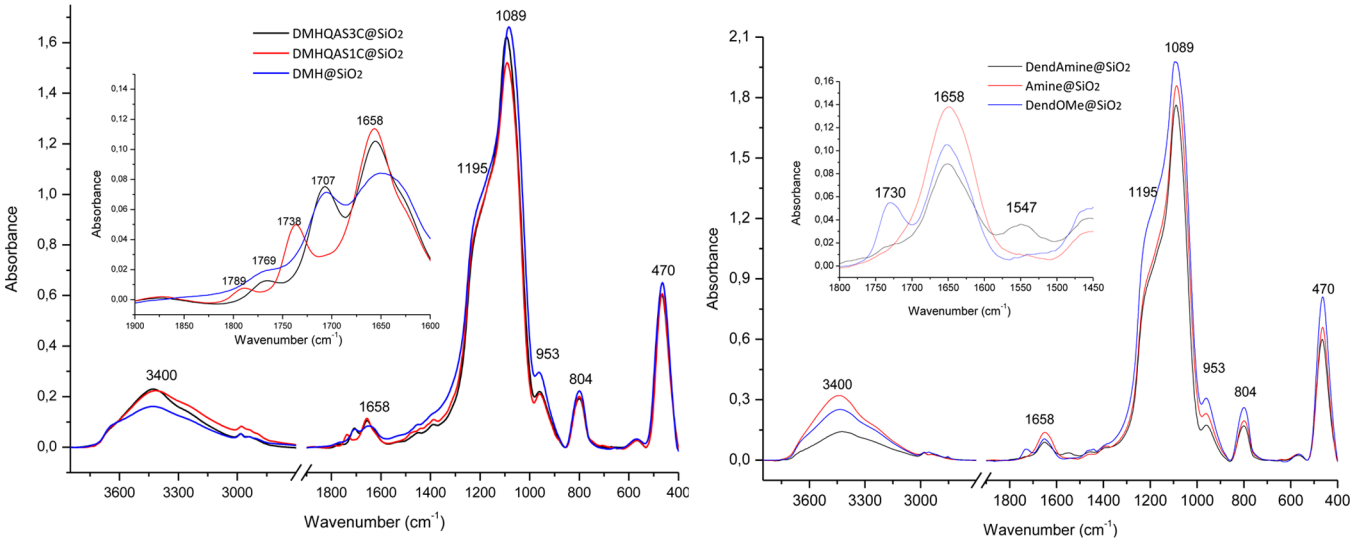

Figure 4. FT-IR spectra of DMH@SiO_2, DMHQAS1C@SiO_2, and DMHQAS3C@SiO_2 (left) and Amine@SiO_2 and DendAmine@SiO_2 (right).

of elements Si, O, C, and Cl. The signal of the Cl element suggests the successful incorporation of CPTES in the structure of a desirable hemispheric shape. This controllable synthesis of hemispherical fragments with intact chloropropyl functional groups would allow for preparing versatile *N*-chloramine-functionalized structures, including DMH@SiO_2, DMHQAS3C@SiO_2, DMHQAS1C@SiO_2, Amine@SiO_2, and DendAmine@SiO_2.

FT-IR spectra were recorded and used for synthesis identification. As shown in Figure 3, SiO_2-coated yeast shows a peak at 3400 cm^{-1} attributed to the stretching vibration of the Si−OH groups. The strong and broad peak at 1089 cm^{-1} and a shoulder peak at 1195 cm^{-1} were assigned to the asymmetric stretching vibration mode of Si−O−Si. The peak at 953 cm^{-1} was attributed to the stretching absorption of Si−OH. The IR peak at 804 cm^{-1} was assigned to Si−O bending vibration, whereas the peak at 470 cm^{-1} was due to Si−O out of plane deformation. These bands were observed in spectra of all prepared samples. Moreover, peaks attributed to the yeast cells were observed at 2956, 2930, 2880, 1658, 1537, 1448, and 1390 cm^{-1}. Yeast cells coated with CPTES showed the same peaks assigned to the yeast cells. Also, a tiny new peak at 700 cm^{-1}, characteristic of C−Cl stretching, appeared in the spectrum of yeast@CPTES/SiO_2@SiO_2. This peak further confirmed the successful incorporation of CPTES in the structure. After the fragmentation and bleaching process, the bands related to the yeast cells dramatically decreased in intensity and some even disappeared. In CPTES fragments, the C−Cl band was still observable, suggesting an intact 3-chloropropyl moiety.

The introduction of *N*-chloramine precursors was carried out in DMF or methanol using CPTES fragments as a starting material (Scheme 2). DMH@SiO_2, DMHQAS1C@SiO_2, DMHQAS3C@SiO_2, and Amine@SiO_2 were synthesized following a nucleophilic reaction in DMF between the CPTES moiety and DMH^-K^+, $(CH_3)_2NCH_2DMH$, $(CH_3)_2N$-$(CH_2)_3DMH$, and ethylendiamine (all prepared beforehand in the laboratory), respectively. Because chlorine was not an ideal leaving group in the nucleophilic substitution, potassium bromide was adopted to catalyze the reaction in the study solutions. DendAmine@SiO_2 was produced by double Michael addition of the amine functions (Amine@SiO_2) on methyl acrylate, followed by amidation of the ester residue using ethylene diamine. As shown in Figure 4, two peaks characteristic of two carbonyl groups in hydantoin were observed at

DOI: 10.1021/acsami.5b02486
ACS Appl. Mater. Interfaces 2015, 7, 11536−11546

Table 1. Chlorine Content in $ClSiO_2$, $ClDMH@SiO_2$, $ClDMHQAS1C@SiO_2$, $ClDMHQAS3C@SiO_2$, $ClAmine@SiO_2$, and $ClDendAmine@SiO_2$ Fragments

fragments	$ClSiO_2$	$ClDMH@SiO_2$	$ClDMHQAS1C@SiO_2$	$ClDMHQAS3C@SiO_2$	$ClAmine@SiO_2$	$ClDendAmine@SiO_2$
$[Cl^+]$ (ppm)	0 ± 117	694 ± 25	576 ± 76	841 ± 88	960 ± 218	2909 ± 200

1707 and 1769 cm^{-1} in the cases of $DMH@SiO_2$ and $DMHQAS3C@SiO_2$ and at 1738 and 1789 cm^{-1} in the case of $DMHQAS1C@SiO_2$. The noticeable shift of $DMHQAS1C@SiO_2$ hydantoin peaks was possibly attributed to the proximity effect of the quaternary ammonium salt to hydantoin in the structure. IR spectra of $Amine@SiO_2$ did not show new observable peaks, probably because the amine feature peaks, such as N−H stretching (3200−3500 cm^{-1}) and C−N stretching (1020−1200 cm^{-1}), were overlapped by the peaks of SiO_2. Nevertheless, a new peak was observed at 1730 cm^{-1} after the Michael double addition, and this was attributed to the methyl ester, suggesting the existence of amine functions in $Amine@SiO_2$. The synthesis of $DendAmine@SiO_2$ by amidation led to the disappearance of the band at 1730 cm^{-1} and the appearance of a band at 1547 cm^{-1}, assigned to amide II.

The activation of antibacterial functions (conversion of N−H to N−Cl) is a crucial step prior to an antimicrobial test; this would permit the loading of oxidative chlorine onto the surface of silica samples. A number of previous studies used sodium hypochlorite at this stage.[12−16] However, Chen et al.[21] compared the chlorination of polymeric hydantoin with bleach and *tert*-butyl hypochlorite and concluded that *tert*-butyl hypochlorite induced better activation of the function and thereby an improved antimicrobial efficacy. Hence, *tert*-butyl hypochlorite was chosen for the chlorination of the samples in this study. After the chlorination process, 5% potassium iodide solution was added dropwise to the dried particle fragments. The successful conversion of N−H to N−Cl was evident through the appearance of a yellow-brownish color ($2I^- + Cl^+ \rightarrow I_2 + Cl^-$) on all functional particles except the silica control. FTIR spectra of the chlorinated functional particle fragments were also collected. Take $DendAmine@SiO_2$ for example, the amide II band from N−H bending disappeared after chlorination (Figure S5 in the Supporting Information), supporting the conversion of N−H to N−Cl. After chlorination, Cl was added in all the denotations for the particle fragments to indicate the structural change. For example, $DMH@SiO_2$ became $ClDMH@SiO_2$ after chlorination. Table 1 shows the results of chlorine loading in different testing samples. SiO_2 fragments showed no chlorine content because of the absence of an active binding site for chloronium ions (Cl^+); $ClDMH@SiO_2$, $ClDMHQAS1C@SiO_2$, and $ClDMHQAS3C@SiO_2$ exhibited 694, 576, and 841 ppm of active chlorine ($[Cl^+]$), respectively. The difference in chlorine concentration in these fragments was mainly attributed to the reactivity of their first material counterparts with the C−Cl band (CPTES particles). Chemically, $(CH_3)_2NCH_2DMH$ possessed a bulky structure with a low degree of freedom, which made its nucleophilic reaction with chloro functional groups on $CPTES/SiO_2@SiO_2$ more difficult than $(CH_3)_2N(CH_2)_3DMH$, as the latter demonstrated more conformational freedom because of the two additional carbons between the tertiary amine and the hydantoin ring. DMH^-K^+ exhibited an intermediate reactivity. The chlorine concentration of $ClAmine@SiO_2$ was higher than those of the fragments cited above, because there were more chlorinable sites in its structure (3 N−H bonds in one molecule). $ClDendAmine@SiO_2$ possesses the highest chlorine value among all of the test materials, attributable to the significant increase of the functionality on the surface of the fragments.

Antimicrobial Assessment. To test the hypothesis that a solid support would be beneficial for antimicrobial properties, we introduced two small organic molecules (Scheme 3) as

Scheme 3. Chemical Structures of Compound 1 (C1) and Compound 2 (C2)

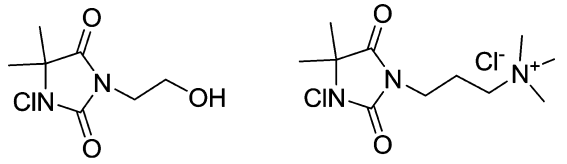

references in the study. Compound 1 (**C1**) carries a hydroxyl group and *N*-chlorohydantoin in its structure, whereas compound 2 (**C2**) carries a quaternary ammonium salt and *N*-chlorohydantoin. Two bacterial stains were chosen as testing models (i.e., typical Gram-negative bacterium *E. coli* and Gram-positive bacterium *B. cereus*). In general, Gram-positive bacteria are more sensitive to *N*-chloramines than Gram-negative bacteria; comparisons between the two strains provide useful information for assessing antibacterial efficacy. To better understand the antimicrobial performance of the synthesized organic molecules and fragments, we also carried out a time-kill study.

Table 2 lists the results collected from the experiment. For reference compounds, **C1** exhibited total kill of *E. coli* and *B. cereus* upon contact for 5 min; **C2** presented a slower kill than **C1** with a 5.4 log reduction of *E. coli* after 10 min and a 5.6 log reduction of *B. cereus* after 40 min. As for the fragments, chlorinated SiO_2 as a control did not demonstrate effective killing of *E. coli* and *B. cereus* even after contact for 2 h. $ClDMH@SiO_2$ exhibited total kill of *E. coli* (5.2 log reduction) and *B. cereus* (5.4 log reduction) after 1 h of contact. $ClDMHQAS1C@SiO_2$ presented a total kill of *E. coli* after 40 min and *B. cereus* after 1 h. $ClDMHQAS3C@SiO_2$ did not exert effective killing of *E. coli* and *B. cereus* at 2 h, but $ClAmine@SiO_2$ exhibited total kill of *E. coli* and *B. cereus* after 2 h. $ClDendAmine@SiO_2$ showed total kill of both *E. coli* and *B. cereus* upon contact for 40 min. The comparative results indicate that small organic molecules were more effective in antimicrobial effectiveness than the fragments in PBS, which might be attributed to higher mobility of the small molecules than the immobilized ones.

In comparison, $ClDMH@SiO_2$ possessed slightly lower reactivity than $ClDMHQAS1C@SiO_2$ against the bacteria, but the effect of positive charge in the molecule was not significantly demonstrated. $ClAmine@SiO_2$ showed effective killing power; its inactivation of bacteria was slower than that of $ClDMH@SiO_2$ and $ClDMHQAS1C@SiO_2$, probably owing to the slower reactivity in amine-based *N*-chloramine than amide-

DOI: 10.1021/acsami.5b02486
ACS Appl. Mater. Interfaces 2015, 7, 11536−11546

Table 2. Antimicrobial Efficacy of Various Fragments and Organic Molecules Against *E. coli* and *B. cereus* in PBS[a]

bacteria	fragments	$[Cl^+]$ (μg/mL)	bacteria log reduction at various contact times (min)					
			5	10	20	40	60	120
Gram-negative *E. coli*	**C1**	20	5.4 ± 0.00	5.4 ± 0.00	5.4 ± 0.00	5.4 ± 0.00	5.4 ± 0.00	5.4 ± 0.00
	C2	20	1.8 ± 0.01	5.4 ± 0.00	5.4 ± 0.00	5.4 ± 0.00	5.4 ± 0.00	5.4 ± 0.00
	$ClSiO_2$	0						0.1 ± 0.13
	ClDMH@SiO_2	20	0.5 ± 0.03	0.4 ± 0.02	0.5 ± 0.06	1.7 ± 0.01	5.2 ± 0.00	5.2 ± 0. 00
	ClDMHQAS1C@SiO_2	20	0.1 ± 0.02	0.1 ± 0.05	1.0 ± 0.02	5.2 ± 0.00	5.2 ± 0.00	5.2 ± 0.00
	ClDMHQAS3C@SiO_2	20	0.3 ± 0.11	0.0 ± 0.13	0.3 ± 0.01	0.6 ± 0.01	1.0 ± 0.02	1.4 ± 0.01
	ClAmine@SiO_2	20	0.1 ± 0.16	0.2 ± 0.34	0.0 ± 0.28	0.1 ± 0.09	0.5 ± 0.02	5.2 ± 0.00
	ClDendAmine@SiO_2	20	0.4 ± 0.08	0.2 ± 0.09	1.2 ± 0.01	5.2 ± 0.00	5.2 ± 0.00	5.2 ± 0.00
Gram-positive *B. cereus*	**C1**	20	5.6 ± 0.00	5.6 ± 0.00	5.6 ± 0.00	5.6 ± 0.00	5.6 ± 0.00	5.6 ± 0.00
	C2	20	0.3 ± 0.06	1.3 ± 0.02	2.5 ± 0.01	5.6 ± 0.00	5.6 ± 0.00	5.6 ± 0.00
	SiO_2	0						0.2 ± 0.09
	ClDMH@SiO_2	20	0.1 ± 0.04	0.1 ± 0.08	0.3 ± 0.07	0.6 ± 0.04	5.4 ± 0.00	5.4 ± 0.00
	ClDMHQAS1C@SiO_2	20	0.3 ± 0.05	0.2 ± 0.13	0.6 ± 0.02	1.0 ± 0.01	5.4 ± 0.00	5.4 ± 0.00
	ClDMHQAS3C@SiO_2	20	0.3 ± 0.03	0.3 ± 0.02	0.4 ± 0.02	0.66 ± 0.01	1.0 ± 0.01	1.6 ± 0.01
	ClAmine@SiO_2	20	0.1 ± 0.09	0.2 ± 0.11	0.3 ± 0.01	0.16 ± 0.14	0.8 ± 0.01	5.4 ± 0.00
	ClDendAmine@SiO_2	20	0.2 ± 0.09	0.4 ± 0.06	1.1 ± 0.01	5.4 ± 0.00	5.4 ± 0.00	5.4 ± 0.00

[a]Inoculum concentration of *E. coli* and *B. cereus* was (1.6−2.5) × 10^5 and (2.4−4.8) × 10^5 CFU/mL, respectively.

Table 3. Antimicrobial Efficacy of Various Fragments and Organic Molecules Against *E. coli* and *B. cereus* in Cell Culture Medium[a]

bacteria	fragments	$[Cl^+]$ (μg/mL)	bacteria log reduction at various contact times (min)					
			20	40	60	120	240	360
Gram-negative *E. coli*	**C1**	20	1.1 ± 0.01	1.1 ± 0.01	1.0 ± 0.02	1.2 ± 0.01	1.8 ± 0.01	1.2 ± 0.01
	C2	20	0.7 ± 0.02	0.5 ± 0.01	0.1 ± 0.05	0.4 ± 0.02	0.6 ± 0.01	0.5 ± 0.03
	SiO_2	0						0.4 ± 0.02
	ClDMH@SiO_2	20	0.1 ± 0.06	0.1 ± 0.22	0.7 ± 0.08	0.8 ± 0.06	2.2 ± 0.01	2.4 ± 0.00
	ClDMHQAS1C@SiO_2	20	0.2 ± 0.06	0.1 ± 0.1	0.8 ± 0.10	2.1 ± 0.01	5.2 ± 0.00	5.2 ± 0.00
	ClDMHQAS3C@SiO_2	20	0.1 ± 0.06	0.1 ± 0.21	0.7 ± 0.01	0.7 ± 0.04	1.4 ± 0.01	1.9 ± 0.01
	ClAmine@SiO_2	20	0.2 ± 0.16	0.2 ± 0.19	0.9 ± 0.03	0.8 ± 0.01	2.0 ± 0.01	5.2 ± 0.00
	ClDendAmine@SiO_2	20	0.0 ± 0.06	0.3 ± 0.06	1.6 ± 0.01	5.2 ± 0.00	5.2 ± 0.00	5.2 ± 0.00
Gram-positive *B. cereus*	**C1**	20	3.2 ± 0.01	2.9 ± 0.01	3.1 ± 0.00	3.2 ± 0.00	3.4 ± 0.00	3.4 ± 0.00
	C2	20	0.0 ± 0.02	0.0 ± 0.06	0.2 ± 0.01	0.00 ± 0.07	0.4 ± 0.02	0.3 ± 0.03
	SiO_2	0						0.73 ± 0.02
	ClDMH@SiO_2	20	0.2 ± 0.14	0.2 ± 0.05	0.2 ± 0.02	0.2 ± 0.03	0.9 ± 0.01	1.8 ± 0.01
	ClDMHQAS1C@SiO_2	20	0.3 ± 0.03	0.3 ± 0.08	0.2 ± 0.07	1.0 ± 0.01	5.4 ± 0.00	5.4 ± 0.00
	ClDMHQAS3C@SiO_2	20	0.2 ± 0.06	0.1 ± 0.02	0.2 ± 0.04	0.2 ± 0.02	1.0 ± 0.01	1.8 ± 0.01
	ClAmine@SiO_2	20	0.1 ± 0.07	0.2 ± 0.02	0.1 ± 0.06	0.1 ± 0.03	1.6 ± 0.01	5.4 ± 0.00
	ClDendAmine@SiO_2	20	0.3 ± 0.06	0.4 ± 0.01	0.5 ± 0.2	0.8 ± 0.01	5.4 ± 0.00	5.4 ± 0.00

[a]Inoculum concentration of *E. coli* and *B. cereus* was (1.6−5.9) × 10^5 and (2.4−3.3) × 10^5 CFU/mL, respectively.

based *N*-chloramine. ClDendAmine@SiO_2 exhibited the highest killing rate among all fragments tested. ClDendAmine@SiO_2 contained the highest density of active chlorine (2909 ppm, Table 1) among all test particles. It was found that the higher the active chlorine density, the more efficient the particles would inactivate the bacteria, as in the case of both ClDMH@SiO_2 and ClAmine@SiO_2, for example (data not shown). Therefore, the highest antibacterial efficacy of ClDendamine@SiO_2 particles was potentially attributed to its highest density of active chlorine, even though the absolute amount of active chlorine used in the antibacterial test was the same for all particles tested. Another possible reason for the higher efficacy was attributed to high fragmentation observed in SEM due to multiple synthesis stages that had made the structure more fragile (Figure S6 in the Supporting Information). On the other hand, ClDMHQAS3C@SiO_2 showed the lowest killing power. This result was not expected. Thus, further studies were carried out to investigate the relationship between surface charge on the fragments and bactericidal activity and is discussed in a later section on zeta potential.

In medical applications such as wound infection control, organic loads and proteins in wound exudates, for instance, are very common and inevitable. To evaluate the antibacterial efficacy of the SiO_2-supported *N*-chloramine biocides in a more realistic condition, a second set of the antimicrobial testing was conducted in the cell culture medium using identical chlorine concentration and bacterial starting inoculum. Because this experiment involved the interaction of the organic load with the chlorine, a competition between the killing and quenching processes would take place and subsequently prolong the rate of bacterial inactivation. Therefore, the study time of this set of experiments was extended from 2 to 6 h. Table 3 summarizes the results obtained.

Compounds **C1** and **C2** did not present a total kill of *E. coli* and *B. cereus*, as had been observed in PBS, even after contact

DOI: 10.1021/acsami.5b02486
ACS Appl. Mater. Interfaces 2015, 7, 11536−11546

for 6 h; this might be attributable to the small molecular size and high mobility of **C1** and **C2**, which would make the quenching process of chlorine in the culture medium more favorable than the killing process. For the fragments, chlorinated SiO_2 as a control did not show effective killing of bacteria in the medium. ClDMH@SiO_2 exhibited a >2 log reduction of *E. coli* and close to 2 log reduction of *B. cereus* after 6 h; the antibacterial efficacy of ClDMH@SiO_2 significantly decreased in culture medium compared to that in PBS because the side reaction of active chlorine with amino acids in the culture medium (chlorine transfer to amine functional groups in amino acids) consumed oxidative chlorine on particle surfaces. ClDMHQAS1C@SiO_2 showed high bacterial killing efficacy (i.e., complete inactivation reached in *E. coli* and *B. cereus* after 4 h, whereas ClAmine@SiO_2 demonstrated complete inactivation in *E. coli* and *B. cereus* after 6 h. Even though the rate of killing in the culture medium was slower than that in PBS, these particles were still considered to be efficient in combating bacteria and achieved total kill in a time frame acceptable for wound infection control. Comparing the antibacterial performance of ClDMH@SiO_2 and ClDMHQAS1C@SiO_2 in the medium, it appeared that the effect of positive charge on antimicrobial efficiency was positive and favorable, whereas the contribution of positive charge in water-soluble *N*-chloramine molecules was negative (**C1** > **C2** in terms of antibacterial potency). Positive charge is capable of contributing to the diffusion of an antibacterial moiety to the proximity of negatively charged bacteria, thus facilitating intimate contact between the two, which is a critical rate-determining step in the inactivation of bacteria by *N*-chloramine-bonded silica particles. However, the rate-limiting step of soluble *N*-chloramine molecules is the penetration of these molecules through the bacterial cell membrane, and neutral molecules were reported to penetrate into bacterial cells better than their charged counterparts.[22]

Conversely, the efficacy of ClDMHQAS3C@SiO_2 against the bacteria in the medium demonstrated similar patterns as in PBS, and its activity was still considered limited. Among all of the test samples, ClDendAmine@SiO_2 was the most efficient fragment, achieving a total kill of *E. coli* after 2 h and *B. cereus* after 4 h.

Zeta potential is a critical parameter that is closely related to particle surface charges. Because one of the objectives in this study was to elucidate the relationship between particle charge and antimicrobial efficiency, experiments were carried out to measure the changes in zeta potential of the test fragments as a function of the medium pH (Figure 5). SiO_2 fragments possessed a high average negative value (approximately −40 ± 6.4 mV) across the tested pH range, indicating high colloidal stability from the anionic repulsions among the particles, because it was reported that colloidal particles with a zeta-potential (absolute value) >30 mV are stable in the suspension.[23] DMH@SiO_2 showed an iso-electrical (IE) point at pH 3.9 but a highly negative profile above pH 7 (−38.7 ± 1.2 mV), suggesting high colloidal stability under neutral conditions because of the negative charge repulsions. DMHQAS1C@SiO_2, DMHQAS3C@SiO_2, Amine@SiO_2, and DendAmine@SiO_2 exhibited IE points at 9.1, 8.6, 8.4, and 9.3, respectively; their profiles below pH 8 were all in the positive range (+30 mV) except for DMHQAS3C@SiO_2 (+14 mV), which is a strong indication of the poor colloidal stability of these particles. It was concluded that DMHQAS1C@SiO_2, Amine@SiO_2, and DendAmine@SiO_2 would be stable under neutral conditions due to positive repulsion, whereas DMHQAS3C@SiO_2 might tend to aggregate because of its low density of positive charges. The *N*-chloramine counterparts of all the particle fragments showed similar zeta potentials to those of their precursors (data not shown).

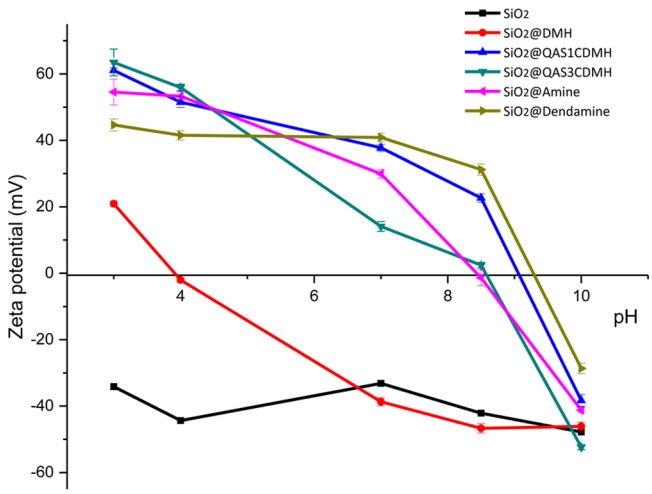

Figure 5. Zeta potential as a function of pH of the different fragments.

Because the antibacterial tests were carried out in PBS (pH 7.4, 0.05 M), zeta potentials of all of the particle fragments were also collected and are presented in Table 4. The increased ionic strength in PBS caused a compression of the electric double layer around all of the particle fragments, leading to decreased zeta potentials (absolute value). However, the general trend was kept the same among all of the particle fragments carrying a positive charge: DendAmine@SiO_2(+) > DMHQAS1C@SiO_2(+) > Amine@SiO_2(+) > DMHQAS3C@SiO_2(+). Again, the *N*-chloramine counterparts of all of the particle fragments showed similar zeta potentials as their precursors.

Table 4. Zeta Potentials of Various Particle Fragments in pH 7.4 PBS

particle fragments	zeta potential (mV)	SD
SiO_2	−23.5	4.6
DMH@SiO_2	−21.1	3.7
DMHQAS1C@SiO_2	15.4	3.5
DMHQAS3C@SiO_2	5.6	1.4
Amine@SiO_2	13.9	1.9
DendAmine@SiO_2	21.7	4.0
ClSiO_2	−23.3	2.9
ClDMH@SiO_2	−20.0	5.1
ClDMHQAS1C@SiO_2	14.1	4.1
ClDMHQAS3C@SiO_2	5.8	1.6
ClAmine@SiO_2	13.3	2.4
ClDendAmine@SiO_2	19.3	2.5

Results obtained from both antibacterial testing and zetametry characterization suggested that colloidal stability was the most important parameter in PBS. ClDMH@SiO_2, ClDMHQAS1C@SiO_2, ClAmine@SiO_2, and ClDendAmine@SiO_2 all demonstrated relatively high colloidal stability in PBS; they also exerted high antimicrobial efficacy in PBS. ClDMHQAS3C@SiO_2 possessed relatively low colloidal stability and as such had limited antimicrobial efficacy. Conversely, antimicrobial efficiency of the test particles in culture medium was affected by numerous factors in addition to

DOI: 10.1021/acsami.5b02486
ACS Appl. Mater. Interfaces 2015, 7, 11536−11546

Table 5. Comparison of Antimicrobial Efficacy of SiO_2@ClAPTES and ClAmine@SiO_2 in PBS and Cell Culture Medium

			bacteria log reduction at various contact times (min)							
medium	bacteria	fragments	5	10	20	40	60	120	240	360
PBS	Gram-negative *E. coli*	SiO_2@ ClAPTES	0.2 ± 0.08	0.1 ± 0.01	0.1 ± 0.06	0.0 ± 0.09	0.2 ± 0.06	2.4 ± 0.00	5.4 ± 0.0	
		SiO_2@ ClAPTES	0.1 ± 0.16	0.2 ± 0.34	0.0 ± 0.28	0.1 ± 0.09	0.5 ± 0.02	5.2 ± 0.00	5.2 ± 0.00	
	Gram-positive *B. cereus*	SiO_2@ ClAPTES	0.2 ± 0.05	0.5 ± 0.12	0.6 ± 0.00	0.6 ± 0.01	0.4 ± 0.00	1.3 ± 0.02	5.7 ± 0.00	
		SiO_2@ ClAPTES	0.1 ± 0.09	0.2 ± 0.11	0.3 ± 0.01	0.16 ± 0.14	0.8 ± 0.01	5.4 ± 0.00	5.4 ± 0.00	
cell culture medium	Gram-negative *E. coli*	SiO_2@ ClAPTES			0.5 ± 0.05	0.3 ± 0.03	0.3 ± 0.01	0.9 ± 0.00	1.5 ± 0.01	0.9 ± 0.01
		SiO_2@ ClAPTES			0.2 ± 0.16	0.2 ± 0.19	0.9 ± 0.03	0.8 ± 0.01	2.0 ± 0.01	5.2 ± 0.00
	Gram-positive *B. cereus*	SiO_2@ ClAPTES			0.0 ± 0.2	0.0 ± 0.02	0.1 ± 0.07	0.8 ± 0.00	0.8 ± 0.01	1.5 ± 0.01
		SiO_2@ ClAPTES			0.1 ± 0.07	0.2 ± 0.02	0.1 ± 0.06	0.1 ± 0.03	1.6 ± 0.01	5.4 ± 0.00

the colloidal stability. The introduction of organic load from culture medium resulted in a competition between the organic load and the bacteria for chlorine from the particles. Although colloidal stability was still critical in correlating to antimicrobial efficacy, surface charges of the fragments, and a positive charge in particular, would play an important role in reactions with bacteria because the bacteria are originally negatively charged (the reported zeta potentials for *E. coli* and *B. cereus* in buffer solution were between −10 and −22 mV^{24-26}). ClDMHQAS1C@SiO_2, ClAmine@SiO_2, and ClDendAmine@SiO_2 all demonstrated acceptable antimicrobial efficacy in the medium, but ClDendAmine@SiO_2 showed the best antimicrobial performance, because in addition to its high colloidal stability and positive charge, it also possessed the highest chlorine density per surface unit among all test samples. The high performance of ClDendAmine@SiO_2 might also be attributable to the higher fragmentation of this sample from multiple synthesis stages. Because Gram-positive bacteria are more sensitive to *N*-chloramines than Gram-negative bacteria, compound **C1** appears to be more effective against Gram-positive *B. cereus* than Gram-negative *E. coli* in the presence of cell culture medium in this study, as shown in Table 3. However, this overall trend is NOT clear for the *N*-chloramine-immobilized particles tested, and further investigation would be needed in the future.

To further confirm the hypothesis that hemispherical particles would enhance the antibacterial effect through their concaved surface relative to that of spherical ones, a supplementary experiment was performed by coating non-broken silica yeast cells with aminopropyltriethoxysilane (SiO_2@APTES) chlorinated with *tert*-butyl alcohol (SiO_2@ClAPTES) followed by testing of its antibacterial efficiency. The resulting particles possessed a chlorine concentration of 8271 ± 92 ppm, higher than that of all other fragments previously tested because of the high amount of APTES incorporated onto the spherical silica surface. Because the APTES coating would remain on the outside of the nonbroken silica particles, the *N*-chloramine generated after chlorination was accessible for both the reducing agent sodium thiosulfate in the chlorine titration experiment and the bacteria in the antibacterial test. The zeta potential of the particles also measured at 33.9 ± 1.25 mV at pH 7, suggesting satisfactory dispersibility. Table 5 summarizes the comparative antibacterial results between SiO_2@ClAPTES and ClAmine@SiO_2, both of which had a similar structure of the active species (*N*-chloramine). SiO_2@ClAPTES showed a slower reactivity than ClAmine@SiO_2 in PBS; it required 4 h to achieve a total kill of *E. coli* and *B. cereus*, which could be accomplished by ClAmine@SiO_2 within 2 h. Similarly, ClAmine@SiO_2 demonstrated more effective killing of the bacteria than SiO_2@ClAPTES in the culture medium. The results indicate that the shape of the particles does play an important role in antimicrobial efficacy, and an increase in the contact surface area of the material with the bacteria would improve the antibacterial performance.

CONCLUSIONS

The concept of hollow hemispherical silica-based structures was designed and prepared in this study; successful incorporation of a functional silane in the structure followed by further chemical modification produced a variety of *N*-chloramine moieties demonstrating the versatility of the materials tested. The antimicrobial properties of these materials were tested against *E. coli* and *B. Cereus* in the presence and absence of an organic load. A correlation between the fragment charge measured by zeta potential and killing efficacy was demonstrated. It was confirmed that quaternary ammonium salt and amine functions enhanced the antimicrobial performance of the materials because of their positive charge. The study also demonstrated that, in the presence of organic load (medium), the positively charged fragments exhibited better performance than small organic molecules. The importance of the particle surface on antimicrobial efficacy was compared on both concave and convex surfaces. The positive contribution of a concave structure to shielding *N*-chloramine from premature quenching by proteins in cell culture medium thus led to enhanced antibacterial outcomes for the particle surface in antimicrobial efficacy. Study results support the use of hollow hemispherical SiO_2 *N*-chloramine biocides as potential antimicrobial agents in medical applications such as wound infection control.

ASSOCIATED CONTENT

Supporting Information

Additional SEM images of silica particles and fragments. ^1H and ^{13}C NMR, MALDI-TOF, and IR spectra of all of the synthesized compounds. The Supporting Information is available free of charge on the ACS Publications website at DOI: 10.1021/acsami.5b02486.

DOI: 10.1021/acsami.5b02486
ACS Appl. Mater. Interfaces 2015, 7, 11536−11546

AUTHOR INFORMATION

Corresponding Author

*Phone: 204-474-9616. Fax: 204-474-7512. E-mail: Song.Liu@umanitoba.ca.

Notes

The authors declare no competing financial interest.

ACKNOWLEDGMENTS

The authors acknowledge financial support from the Canadian Institutes of Health Research (CIHR) and the Natural Sciences and Engineering Research Council of Canada (NSERC) by a Collaborative Health Research Projects (CHRP) Operating Grant (Grant No. CHRP 413713-2012) and a Discovery Grant (Grant No. RGPIN/04922-2014).

REFERENCES

(1) Cohen, M. L. Changing Patterns of Infectious Disease. *Nature* **2000**, *406*, 762−767.

(2) Gold, H. S.; Moellering, R. C. Antimicrobial-drug Resistance. *N. Engl. J. Med.* **1996**, *335*, 1445−1453.

(3) Walsh, C. Molecular Mechanisms that Confer Antibacterial Drug Resistance. *Nature* **2000**, *406*, 775−781.

(4) Gottardi, W.; Debabov, D.; Nagi, M. *N*-Chloramines, a Promising Class of Well-Tolerated Topical Anti-Infectives. *Antimicrob. Agents Chemother.* **2013**, *57*, 1107−1114.

(5) Ahmed, A. E. S.; Hay, N. J.; Bushell, E. M.; Wardell, J. N.; Cavalli, G. Macroscopic *N*-Halamine Biocidal Polymeric Beads. *J. Appl. Polym. Sci.* **2010**, *116*, 2396−2408.

(6) Dong, A.; Huang, J.; Lan, S.; Wang, T.; Xiao, L.; Wang, W.; Zhao, T.; Zheng, X.; Liu, F.; Gao, G.; Chen, Y. Synthesis of *N*-Halamine-Functionalized Silica−Polymer Core−Shell Nanoparticles and Their Enhanced Antibacterial Activity. *Nanotechnology* **2011**, *22*, 295602.

(7) Dong, A.; Lan, S.; Huang, J.; Wang, T.; Wang, W.; Xiao, L.; Zheng, X.; Liu, F.; Gao, G.; Chen, Y. Preparation of Magnetically Separable *N*-Halamine Nanocomposites for the Improved Antibacterial Application. *J. Colloid Interface Sci.* **2011**, *364*, 333−340.

(8) Borovička, J.; Metheringham, W. J.; Madden, L. A.; Walton, C. D.; Stayanov, D. S.; Paunov, V. N. Photothermal Colloid Antibodies for Shape-Selective Recognition and Killing of Microorganisms. *J. Am. Chem. Soc.* **2013**, *135*, 5282−5285.

(9) Borovička, J.; Stayanov, D. S.; Paunov, V. N. Shape Recognition of Microbial Cells by Colloidal Cell Imprints. *Nanoscale* **2013**, *5*, 8506−8568.

(10) Tang, F.; Li, L.; Chen, D. Mesoporous Silica Nanoparticles: Synthesis, Biocompatibility and Drug Delivery. *Adv. Mater.* **2012**, *24*, 1504−1534.

(11) Jal, P. K.; Patel, S.; Mishra, B. K. Chemical Modification of Silica Surface by Immobilization of Functional Groups for Extractive Concentration of Metal Ions. *Talanta* **2004**, *62*, 1005−1028.

(12) Dong, A.; Zhang, Q.; Wang, T.; Wang, W.; Liu, F.; Gao, G. Immobilization of Cyclic *N*-Halamine on Polystyrene-Functionalized Silica Nanoparticles: Synthesis, Characterization, and Biocidal Activity. *J. Phys. Chem. C* **2010**, *114*, 17298−17303.

(13) Dong, A.; Lan, S.; Huang, J.; Wang, T.; Zhao, T.; Xiao, L.; Wang, W.; Zheng, X.; Liu, F.; Gao, G.; Chen, Y. Modifying Fe_3O_4-Functionalized Nanoparticles with *N*-Halamine and Their Magnetic/Antibacterial Properties. *ACS Appl. Mater. Interfaces* **2011**, *3*, 4228−4235.

(14) Liang, J.; Barnes, K.; Akdag, A.; Worley, S. D.; Lee, J.; Broughton, R. M.; Huang, T. S. Improved Antimicrobial Siloxane. *Ind. Eng. Chem. Res.* **2007**, *46*, 1861−1866.

(15) Liang, J.; Owens, J. R.; Huang, T. S.; Worley, S. D. Biocidal Hydantoinyl Siloxane Polymers. IV. *N* Halamine Siloxane-Functionalized Silica Gel. *J. Appl. Polym. Sci.* **2006**, *101*, 3448−3454.

(16) Barnes, K.; Liang, J.; Worley, S. D.; Lee, J.; Broughton, R. M.; Huang, T. S. Modification of Silica Gel, Cellulose, and Polyurethane with a Sterically Hindered *N*-Halamine Moiety to Produce Antimicrobial Activity. *J. Appl. Polym. Sci.* **2007**, *105*, 2306−2313.

(17) Kloth, L. C.; Berman, J. E.; Laatsch, L. J.; Kirchner, P. A. Bactericidal and Cytotoxic Effects of Chloramine-T on Wound Pathogens and Human Fibroblasts In Vitro. *Adv. Skin Wound Care* **2007**, *20*, 331−345.

(18) Gottardi, W.; Klots, S.; Nagl, M. Superior Bactericidal Activity of *N*-Bromine Compounds Compared to Their *N*-Chlorine Analogues Can Be Reversed under Protein Load. *J. Appl. Microbiol.* **2014**, *116*, 1427−1437.

(19) Li, L.; Pu, T.; Zhanel, G.; Zhao, N.; Ens, W.; Liu, S. New Biocide with Both *N*-Chloramine and Quaternary Ammonium Moieties Exerts Enhanced Bactericidal Activity. *Adv. Healthcare Mater.* **2012**, *1*, 609−620.

(20) Akdag, A.; Okur, S.; McKee, M. L.; Worley, S. D. The Stabilities of N−Cl Bonds in Biocidal Materials. *J. Chem. Theory Comput.* **2006**, *2*, 879−884.

(21) Chen, Y.; Wang, L.; Yu, H.; Shi, Q.; Dong, X. Synthesis, Characterization, and Antibacterial Activities of Synthesis, Characterization, and Antibacterial Activities of Novel *N*-Halamine Copolymer. *J. Mater. Sci.* **2007**, *42*, 4018−4024.

(22) Wang, L.; Belisle, B.; Bassiri, M.; Xu, P.; Debabov, D.; Celeri, C.; Alvarez, N.; Robson, M. C.; Payne, W. G.; Najafi, R.; Khosrovi, B. Chemical Characterization and Biological Properties of NVC-422, A Novel, Stable *N*-Chlorotaurine Analog. *Antimicrob. Agents Chemother.* **2011**, *55*, 2688−2692.

(23) Hanaor, D.; Michelazzi, M.; Leonelli, C.; Sorrell, C. C. The Effects of Carboxylic Acids on the Aqueous Dispersion and Electrophoretic Deposition of ZrO_2. *J. Eur. Ceram. Soc.* **2012**, *32*, 235−244.

(24) Ankolekar, C.; Labbe, R. G. Physical Characteristics of Spores of Food-Associated Isolates of the *Bacillus cereus* Group. *Appl. Environ. Microbiol.* **2010**, *76*, 982−984.

(25) Lemos, M.; Borges, A.; Teodósio, J.; Araújo, P.; Mergulhão, F.; Melo, L.; Simões, M. The effects of ferulic and salicylic acids on *Bacillus cereus* and *Pseudomonas fluorescens* single- and dual-species biofilms. *Int. Biodeterior. Biodegrad.* **2014**, *86*, 42−51.

(26) Alves, C. S.; Melo, M. N.; Franquelim, H. G.; Ferre, R.; Planas, M.; Feliu, L.; Bardaji, E.; Kowalczyk, W.; Andreu, D.; Santos, N. C.; Fernandes, M. X.; Castanho, M. A. *Escherichia coli* Cell Surface Perturbation and Disruption Induced by Antimicrobial Peptides BP100 and pepR*. *J. Biol. Chem.* **2010**, *285*, 27536−27544.

DOI: 10.1021/acsami.5b02486
ACS Appl. Mater. Interfaces 2015, 7, 11536−11546